ELSEVIER

CrossMark

BRACHYTHERAPY

Brachytherapy 16 (2017) 421–432

Physics

A directional ^{103}Pd brachytherapy device: Dosimetric characterization and practical aspects for clinical use

Mark J. Rivard*

Department of Radiation Oncology, Tufts University School of Medicine, Boston, MA

ABSTRACT

PURPOSE: A brachytherapy (BT) device has been developed with shielding to provide directional BT for preferentially irradiating malignancies while sparing healthy tissues. The CivaSheet is a flexible low-dose-rate BT device containing CivaDots with ^{103}Pd shielded by a thin Au disk. This is the first report of a clinical dosimetric characterization of the CivaSheet device.

METHODS AND MATERIALS: Radiation dose distributions near a CivaDot were estimated using the MCNP6 radiation transport code. CivaSheet arrays were also modeled to evaluate the dose superposition principle for treatment planning. The resultant data were commissioned in a treatment planning system (TPS) (VariSeed 9.0), and the accuracy of the dose superposition principle was evaluated for summing individual elements comprising a planar CivaSheet.

RESULTS: The dose-rate constant (0.579 cGy/h/U) was lower than for ^{103}Pd seeds due to Au L-shell x-rays increasing the air-kerma strength. Radial dose function values at 0.1, 0.5, 2, 5, and 10 cm were 1.884, 1.344, 0.558, 0.088, and 0.0046, respectively. The two-dimensional anisotropy function exhibited dramatic reduction between the forward (0°) and rearward (180°) directions by a factor of 276 at $r = 0.1$ cm, 24 at $r = 1$ cm, and 5.3 at $r = 10$ cm. This effect diminished due to increasingly scattered radiation. The largest gradient in the two-dimensional anisotropy function was in contact with the device at 92° due to the Au disk shielding. TPS commissioning and dose superposition accuracies were typically within 2%.

CONCLUSIONS: Simulations of the CivaDot yielded comprehensive dosimetry parameters that were entered into a TPS and deemed acceptable for clinical use. Dosimetry measurements of the CivaSheet are also of interest to the BT community.

Keywords: Monte Carlo methods; Dosimetry; CivaSheet

Introduction

Brachytherapy (BT) sources have historically been designed with the goal of having an isotropic dose distribution. The first radionuclides, that is, ^{226}Ra and ^{222}Rn (1), were high-energy photon emitters that intrinsically provided more uniform dose distributions than low-energy (≤50 keV) photon emitters (2, 3). Even with low-Z titanium encapsulation and careful endwelds to seal the source, conventional low-energy BT sources exhibit substantial dose anisotropy as the radionuclide is usually deposited on or adjacent to the radio-opaque marker (4, 5), exacerbating the dose anisotropy due to source self-shielding. Although dose anisotropy for a single source does not correspond to dose uniformity for a volumetric implant, it has been shown that sources with less dose anisotropy can improve target dose uniformity while minimizing the irradiation of adjacent healthy tissues (6). Taking this concept further, elongated sources have been developed (7, 8) to address dose uniformity for volumetric targets.

Directional sources can address the challenge of balancing sufficient irradiation of the target while protecting healthy tissues. High-dose-rate (HDR) sources containing ^{153}Gd (9) or ^{192}Ir (10, 11) with built-in shielding have been investigated, but current technology prohibits interstitial implantation due to the required shield thickness and resultant puncture diameter. A directional source is more readily achieved with a source having lower energy emissions and consequently a thinner shield. Thomadsen *et al.*

Received 29 September 2016; received in revised form 10 November 2016; accepted 29 November 2016.

* Corresponding author. Department of Radiation Oncology, Tufts University School of Medicine, 800 Washington Street, Boston, MA 02111. Tel.: +1-508-497-9498.

E-mail address: markjrivard@gmail.com.

1538-4721/$ - see front matter
http://dx.doi.org/10.1016/j.brachy.2016.11.011

researched this for low-dose-rate (LDR) ^{125}I seeds having a built-in Au shield where a dose reduction of 10–15 times lower was reported and substantial dose conformity for theoretical breast implants was observed (12, 13). The source design was not cylindrically symmetric and required affixing the sources within the patient to prevent the undesirable circumstance where the healthy tissue is irradiated to full dose, while the targeted tissue is protected.

To address these challenges, a low-energy BT device was developed that permits permanent implantation using sources with fixed orientation within the patient. The CivaSheet (CivaTech Oncology, Inc., Durham, NC) is a flexible LDR BT device containing CivaDots with ^{103}Pd shielded by a thin Au disk. The coin-shaped CivaDots are placed in a grid-like array within a flexible polymer base. In this way, the mesh-like device provides irradiation on one side yet protects tissues on the shielded side. This is not possible with a conventional mesh containing seeds in strands.

Being a novel BT device, research was necessary to permit widespread clinical use with image-guided treatment planning. The American Association of Physicists in Medicine (AAPM) has set standards for dosimetric characterization and the calibrations of new BT sources (4, 14, 15). Although the calibration aspects have been recently addressed by Aima *et al.* (16), there still was a need for clinics to have the necessary dosimetric information to facilitate treatment planning. Therefore, it was the primary objective of the current study to present a comprehensive dosimetric characterization for the CivaSheet device.

Methods

Monte Carlo simulations

Monte Carlo radiation transport simulations were performed using version 1.0 of the MCNP6 code (17). The author has BT dosimetry experience with this user code (18), recently for ^{103}Pd sources (8, 19), and also with MCNP6 (20). In general, the simulation approach described in detail by Rivard for BT sources was followed (21). Toward specifying the methodologic details required by the 2004 AAPM TG-43U1 report, photon transport was performed using the MCNP6 mcplib12p cross-section library based on the Evaluated Nuclear Data File/B version VI Release 8 ENDF/B-VI.8 (22) in conjunction with the ^{103}Pd photon spectrum from the National Nuclear Data Center (23) based on the evaluation by De Frenne (24), which included the 2.7 keV L-shell characteristic x-ray.

Absorbed dose was determined from the MCNP6 track-length estimator to convert photon fluence to collisional kerma using water or tissue (25) mass-energy absorption coefficients (26) from the National Institute of Standards and Technology (NIST). To determine the BT dosimetry parameters, photon transport was performed in water with the default 1 keV low-energy cutoff and 3.4×10^{10} photon histories. For determination of Monte Carlo–derived air-kerma strength s_K to estimate the dose-rate constant Λ (27), several low-energy thresholds were used. Specifically, influence of 2.7 keV Pd L-shell x-rays, Au L-shell x-rays from the shielding disk, and ^{103}Pd gamma rays greater than 40 keV were ascertained in addition to the standard 5 keV low-energy cutoff. The number of photon histories was 7.7×10^9 for the in vacuo simulations.

Source and phantom geometry

The CivaSheet is a flexible device containing the radioactive CivaDots sandwiched between two layers of 0.0125 cm thick polymer ($H_7C_5O_3$, $\rho = 1.20$ g/cm^3). Circular fenestrations (0.318 cm diameter) in the polymer are positioned with 0.8 cm spacing along a square grid, which alternate with the CivaDots that are also spaced with a (0.8 cm)^2 square grid. The fenestrations serve as anchor points to facilitate surgical placement and to provide fluid transport across the device. The CivaSheet comes in two sizes, 6×12 or 6×18 arrays of 72 or 108 CivaDots, respectively. Source strength is uniform across all CivaDots in an array as the prescription depth is typically constant and the dose at any point close to the CivaSheet is dominated by CivaDots in close proximity.

The CivaDot is manufactured as a plastic ($C_{12}H_{10}O_3$, $\rho = 1.30$ g/cm^3) disk that is 0.0536 cm high and 0.253 cm in diameter and contains a circular depression (2.4×10^{-5} cm^3) filled with ^{103}Pd. This depression is covered with a thin (0.005 cm) Au disk (19.3 g/cm^3) that is 0.185 cm in diameter and then sealed with a polymer ($C_{64}H_{95}N_3O_{18}$ $\rho = 1.06$ g/cm^3) to be flush with the plastic disk (Fig. 1). The dimensions were taken from the average of 10 samples of manufactured CivaDot components. Measurements were performed using micrometers, calipers, and cylindrical tools with comparison to dimensional standards (28), having an accuracy of about 0.005 cm (0.002″) and an uncertainty ($k = 2$) of 0.005 cm (0.002″). The source active length was set to zero as the depression depth was only

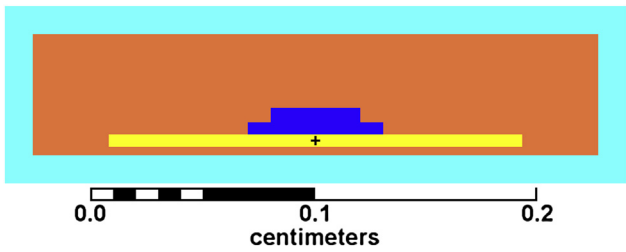

Fig. 1. Cross-sectional view of the cylindrically symmetric CivaDot ^{103}Pd directional low-dose-rate BT source, which is a component of the CivaSheet BT device. The light blue peripheral region is a portion of the flexible polymer base containing the CivaDot. The orange region is the plastic disk (0.253 cm diameter) housing the depression containing the active region (dark blue) that is shielded by a 0.005-cm thick Au disk (yellow). The crosshair centered in the Au disk depicts the coordinate system origin centered on the radio-opaque marker. The unshielded direction is on top, whereas the CivaDot backside is toward the bottom. BT = brachytherapy. (For interpretation of the references to color in this figure legend, the reader is referred to the Web version of this article.)

0.012 cm, and the dose distribution was not expected to have a prolate shape as would be corrected for with a line-source geometry function oriented along the source axis of symmetry.

Based on the range of clinical prescriptions and subsequent customer orders of source strength, the amount of Pd solution containing ^{103}Pd is variable within the CivaDot depression. For delivery of 60 Gy to a depth of 0.5 cm from a CivaSheet 6 × 6 array, a nominal loading of 160 Ci/g ^{103}Pd is necessary at the time of manufacture. This yields approximately 120 Ci/g at the time of implant and 60 Ci/g after one half-life for a permanent implant, which corresponded to approximately 35% Pd by mass with ρ = 1.599 g/cm^3. Therefore, a ^{103}Pd loading of 60 Ci/g (also with the presence of stable Pd and the ^{103}Pd decay product of Rh) was contained within the CivaDot depression and assumed to be of uniform physical distribution. As suggested by Aima *et al.* (16), a range of additional loadings were also examined to glean the influence of this variable on the resultant CivaDot dose distribution and the related BT dosimetry parameters.

CivaDots are contained within a flexible, low-Z ($C_5H_7O_3$) polymer base having ρ = 1.20 g/cm^3 and a 0.0125 cm thickness. A single CivaDot was simulated within the polymer base with a resultant overall height of 0.0786 cm and diameter of 0.2780 cm. In practice, the lateral extent of the plastic base continues on to the next CivaDot (positioned in a square grid with 0.8 cm center-to-center spacings); however, the base dimensions were constrained for the purpose of determining single-source BT dosimetry parameters. The CivaDot and plastic base were centered in a 60-cm sphere of water (ρ = 0.998 g/cm^3) for evaluating dose. This permitted at least 17.5 cm of backscatter for $r \leq$ 12.5 cm, which was necessary for accurate estimates of dose at large distances where the ^{103}Pd gamma rays have a maximum energy of 497 keV (2, 29). Using a polar coordinate system, dose was estimated in 0.0002-cm-thick radial bins from 0.025 cm to 0.15 cm in 0.025 cm increments, 0.2 cm and 0.25 cm, then 0.3 cm–12.5 cm in 0.1 cm increments. The angular distribution in water was estimated from $0° \leq \theta \leq 180°$ in 1° increments. In this way, the dose distribution for a CivaDot was simulated and the BT dosimetry parameters were then determined. For estimating s_K, the CivaDot and plastic base were positioned 30 cm from an 8-cm-diameter aperture sampling space in vacuum. This method is used at NIST, which includes the plastic base to hold the CivaDot static while performing the measurements (16) and is part of the source holder for independent calibrations of source strength as performed by the clinical medical physicist (14, 30).

The coordinate system origin for the CivaDot was positioned at the center of the Au shielding disk because this is the identifiable position of the CivaDot during CT-based image-guided BT treatment planning, and the center-of-mass position for the Pd differs by only 0.007 cm from the Au disk center. The two-dimensional (2D) dose calculation formalism in the AAPM TG-43 protocol orients the axis of symmetry along the source long axis for low-energy photon-emitting seeds. The axis of symmetry is along the short axis for the disk-shaped CivaDot, which is oblate instead of prolate-like seeds. The CivaDot does not exhibit mirror symmetry on the transverse plane, so dose characterization was necessary for supplementary angles where $\theta = 0°$ was defined in the unshielded direction and $\theta = 180°$ was on the CivaDot backside. The TG-43 protocol was developed for cylindrically shaped BT sources that manifest small changes in dose along the transverse plane (i.e., $\theta = 90°$). However, it was anticipated that there would be a significant dose gradient for the CivaDot near $\theta = 90°$ due to the Au disk shielding as previously examined for other BT sources (31). Therefore, the radial dose function $g_{MC}(r)$ was defined along $\theta_0 = 0°$, and the 2D anisotropy function $F_{MC}(r,\theta)$ was normalized along this axis of symmetry. It was expected that the dose gradient would be minimal along 0°, so the value of s_K was estimated along the axis of symmetry as established at NIST using the wide-angle free-air chamber (WAFAC) and transferred to Accredited Dosimetry Calibration Labs for calibration of instrumentation such as clinic well chambers (16).

TPS commissioning

CivaDot dose distributions were assumed to be cylindrically symmetric and were obtained over a 2D grid with 131 radial and 181 angular points. Excluding locations within the CivaDot and correcting for the geometry function (i.e., inverse square), this $F_{MC}(r,\theta)$ grid totaled 23,309 data points. For entry into a clinical treatment planning system (TPS), this data set would requiring thinning. The BT dosimetry parameters were reduced to 38 radial and 38 angular points for $F_{TPS}(r,\theta)$ entry into the VariSeed 9.0 TPS (Varian Medical Systems, Inc. in Palo Alto, CA) in the supplemental files (Supplementary File 1). The entered radii were 0.075, 0.1, 0.125, 0.15, 0.2, 0.25 cm, 0.3–1.0 cm in 0.1 cm increments, 1.2 cm, and 1.5–12.5 cm in 0.5 cm increments. The angles were 0°–80° in 10° increments, 85°, 87°–100° in 1° increments, 103°, 105°–150° in 5° increments, 160°, 170°, and 180°. Similarly, the 131 $g_{MC}(r)$ data points spanning $0.075 \leq r \leq 12.5$ cm were reduced to the aforementioned 38 radii as used for $F_{TPS}(r,\theta)$. In this way, linear and bilinear fitting for $g_{TPS}(r)$ and $F_{TPS}(r,\theta)$, respectively, produced interpolation errors <2% (typically within 1%) as required by the AAPM (4, 32).

Another aspect pertinent to commissioning the source in the TPS was entry of irregular values for the conversion factor for apparent activity (A_{app}) to S_K, source length, 2D anisotropy function, and the one-dimensional anisotropy function. As recommended by the AAPM (33), the CivaSheet manufacturer does not work with the antiquated units of A_{app} anywhere in their processes, yet the TPS requires entry of a nonzero value. To minimize likelihood

for human error in confusing A_{app} and S_K during clinical treatment planning (34), a value of 0.2 U/mCi was entered vs. the near-unity value of 1.297 U/mCi as previously used for ^{103}Pd seeds (35). Values of zero also cannot be entered into VariSeed for the active length or the 2D anisotropy function, so the smallest permissible values were entered, 0.001 cm and 0.0001 cm, respectively. However, a physical length of 0.4 cm was entered to give the appearance of length to the CivaDot to permit source rotation for orienting an individual CivaDot to follow the shape of the flexible CivaSheet following implantation. Values for the 1D anisotropy function were set to a constant of 0.1, and the ''factors'' and ''constant'' anisotropy corrections in VariSeed were not checked-off for source commissioning.

Evaluation of dose superposition

To characterize the CivaSheet dose distribution as a combination of CivaDots for practical treatment planning (36), tests of the suitability of single-source dose superposition were made in a similar manner as that previously reported (8). Specific to the CivaSheet, 6 × 6, 6 × 12, and 6 × 18 arrays of CivaDots were modeled and the dose distributions were compared to those obtained from the sum of individual CivaDots located at the same positions as in the arrays. Dose distributions were examined in an absolute manner as well as their ratios, and results at locations within the device were excluded. Dose distributions were estimated with rectilinear meshes having $(0.05\ \text{cm})^3$ voxels and spanning a range of 12.5 cm. The CivaSheet simulations included the fenestrations present in the flexible polymer base used to facilitate surgical placement, described as a bioabsorbable membrane in Fig. 1 of Aima et *al.* (16).

Uncertainty analysis for single-source dose calculations

As recommended by the 2004 AAPM TG-43U1 report (4), a detailed uncertainty analysis is presented to assess statistical (Type A) and nonstatistical uncertainties (Type B) for their contributions to BT dosimetry parameters according to the TG-138 report (37). The focus is on estimating the uncertainty in dose calculations at depths of 0.5 cm and 1.0 cm as well as for $g_{MC}(0.5\ \text{cm})$, s_K, and Λ. For brevity, details are given only for some of the uncertainty components because the majority of the items have been previously examined for the ^{103}Pd CivaString and were assumed to be applicable to the ^{103}Pd CivaSheet (8).

The contents of CivaDots are fixed and not subject to change following adjustment of their orientation. The Au disk is placed in mechanical contact with surfaces within the CivaDot plastic disk. Evaluation of the measured samples indicated that variations in the depth of the ^{103}Pd depression were within the measurement uncertainty. The only issue examined for this uncertainty component was the variation in ^{103}Pd loading based on variations required for customer orders. When altering the ^{103}Pd loading from 35% to either 20% or 50% (encompassing the majority of prescription doses), the $\dot{d}$ (0.5 cm, 0°) value changed by +2.9% or −3.8%, respectively, for a mean variation of 3.4%. Changes in the $\dot{d}$ (1.0 cm, 0°) value over the same range were less (+2.4% or −3.4%) with a mean variation of 2.9%. However, these changes largely canceled out for derivation of $g_{MC}(0.5\ \text{cm})$ and amounted to +0.53% and −0.45% for a mean variation of 0.49%. Changes in ^{103}Pd loading influenced s_K and Λ more so with mean variations of 5.8% and 2.9%, respectively. These uncertainties (and those applicable from the ^{103}Pd CivaString analysis) are presented in Table 1.

Results

The CivaDot photon spectrum with a 35% Pd loading in vacuum revealed the principal ^{103}Pd x-rays as well as the complex excitations from the Au disk (Fig. 2).

A value of $\Lambda = 0.579 \pm 0.017$ cGy h^{-1} U^{-1} was obtained for 35% Pd loading, which varied from 0.563 to 0.596 cGy h^{-1} U^{-1} for Pd loadings of 20% and 50%, respectively (Supplementary File 1). These changes were mainly influenced by s_K changes where lower loadings produced higher Λ values. This was expected from the inverse relationship of $\Lambda = \dot{d}\ (1.0\ \text{cm}, 0°)/s_K$. Relative to the reference position, the dose rate in contact with the CivaSheet was 370 cGy h^{-1} U^{-1} in the forward (0°) direction and 1.2 cGy h^{-1} U^{-1} in the rearward (180°) direction.

The $g_{MC}(r)$ values followed monotonic behavior, decreasing from a value of nearly two at $r = 0.075$ cm to a value < 0.005 at $r = 10$ cm. Beyond approximately 10 cm, the diminishment rate of g_{MC} values decreased as contributions from higher-energy ^{103}Pd gamma rays became increasingly important. In comparison to the reference 35% Pd loading (Fig. 3), the g_{MC} values for Pd loadings of 20% and 50% differed by 3% only for the closest distances, that is, $r \le 0.1$ cm (Supplementary File 1). Otherwise, the ratio of $g_{MC}(r)$ results was nearly insensitive to the amount of Pd loading.

Defined as unity at $\theta = 0°$, the $F_{MC}(r,\theta)$ results were greater than 0.95 for $0° \le \theta \le 45°$ and changed only slightly with increasing radius (Fig. 4). There was a steep gradient at $p(0.15\ \text{cm}, \theta = 92°)$ where the dose rate in water was 3.2 times lower than at $p(0.15\ \text{cm}, \theta = 91°)$. The dose gradient diminished with increasing distance due to proportionately larger contributions of radiation scatter. Similarly, the ratio of dose rates for the unshielded to shielded sides for a single CivaDot diminished from a factor of 270 at $r = 0.1$ cm, 36 at $r = 0.5$ cm, 23 at $r = 1$ cm, and 5.1 at $r = 10$ cm. Even with increased tangential attenuation through the Au foil for $100° \le \theta \le 180°$, the $F_{MC}(r,\theta)$ values for a given radius were lowest at $\theta = 180°$. In comparison to the reference loading of 35% Pd, $F_{MC}(r,\theta)$ results for Pd loadings of 20% or 35% remained constant within 1% for $\theta \le 42°$ over all radii and maximally changed by +6.4% and −8.3%, respectively, at

Table 1
Standard uncertainties ($k = 1$) for components of the Monte Carlo simulations for the CivaSheet^{103}Pd source (i.e., CivaDot) with a 35% Pd loading

	$\dot{d}$(0.5 cm, 0°)		$\dot{d}$(1.0 cm, 0°)		g_{MC}(0.5 cm)		s_K		Λ	
Uncertainty component	Type A	Type B	Type A	Type B	Type A	Type B	Type A	Type B	Type A	Type B
Source design		3.4		2.9				5.8		2.9
Dynamic internal components										
Source photon spectrum		0.005		0.006				0.012		0.014
Phantom composition		0.04		0.08		0.09		0.003		0.8
Monte Carlo code physics		0.1		0.1				0.1		
μ_{en}/ρ for dose calculation	0.07	0.87	0.07	0.87			0.07	0.80		
μ/ρ for phantom attenuation		0.31		0.61		0.69				0.61
Tally volume averaging		<0.0001		<0.0001				<0.0001		
Tally statistics	0.01		0.01		0.01		0.02		0.02	
Quadrature sum	0.07	3.51	0.07	3.09	0.01	0.69	0.07	35.85	0.02	2.96
Total standard uncertainty	3.5		3.1		0.7		5.9		3.0	

All values are expressed as percentages.

p(1.0 cm, $\theta = 90°$) and p(0.6 cm, $\theta = 89°$) in close proximity where radiation scatter contributions were relatively low (Supplementary File 1).

TPS commissioning of a single source (i.e., CivaDot)

After distillation of the Monte Carlo reference (35% Pd loading) data into a new data set for entry into the VariSeed 9.0 TPS for commissioning, hand calculations based on the 2D TG-43 formalism generally indicated good agreement with the TPS output. Specifically, the ratio of the TPS results to the hand calculations for water were within 2% (1.3% $k = 1$) of unity for 90 of 91 data points, except at one position p(4.1 cm, $\theta = 90°$) where the ratio was 1.031 (the $k = 1$ Monte Carlo statistical uncertainties at this location were 0.04%). While near the 2% threshold set by the AAPM (4, 32) , this value was categorized as an outlier given the challenges for users to manually position dose points within VariSeed using a mouse and not quantitatively entering dose point locations via a keypad. The estimated positioning accuracy for manually positioned dose points was <0.1 cm, which fit with the calculated dose deviation for this single dose point. Therefore, the dose distribution for a CivaDot was successfully commissioned within the VariSeed 9.0 TPS (Fig. 5).

For comparison, the Monte Carlo data based on dose to tissue in tissue were similarly distilled and entered into the VariSeed 9.0 TPS, which were generally similar to the dose to water in water results. For $r \leq 0.8$ cm, the dose ratios were within 2% of unity and the dose rate at p(1 cm, $\theta = 0°$) in tissue was 2.2% lower than in water. For increasing distance, the tissue was more attenuating and the dose ratio decreased to a minimum 0.66 at p(9.5 cm, $\theta = 23°$).

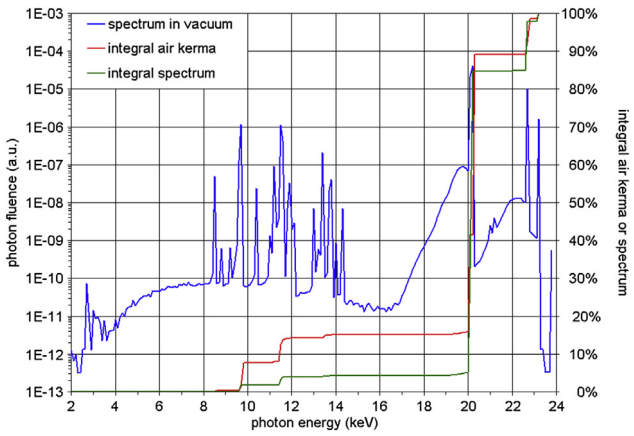

Fig. 2. Based on the NIST WAFAC geometry, the photon spectrum of the CivaDot (blue curve) was estimated using the MCNP6 radiation transport code with fluence results expressed in native units (MeV/g/history) for 35% Pd loading. The principal x-rays generated following ^{103}Pd source disintegration occur at 20 and 23 keV, and the weak emission at 2.7 keV was observed. Also evident were the numerous Au L-shell characteristic x-rays from 8 to 15 keV (principally 9.7 keV and 11.5 keV), which contributed to the total air-kerma strength (red curve) and the total number of photons (green curve) by approximately 15% and 4%, respectively. NIST = National Institute of Standards and Technology; WAFAC = wide-angle free-air chamber. (For interpretation of the references to color in this figure legend, the reader is referred to the Web version of this article.)

Dose superposition principle

Compared to multisource CivaSheet array, dose superposition of CivaDots replicated the dose distribution within

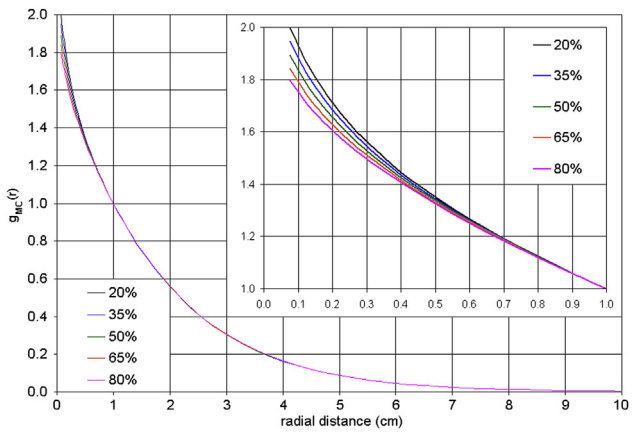

Fig. 3. Behavior of Monte Carlo–derived radial dose function results using the point-source geometry function as a function of the percentage of Pd loading in the active region inside a CivaDot.

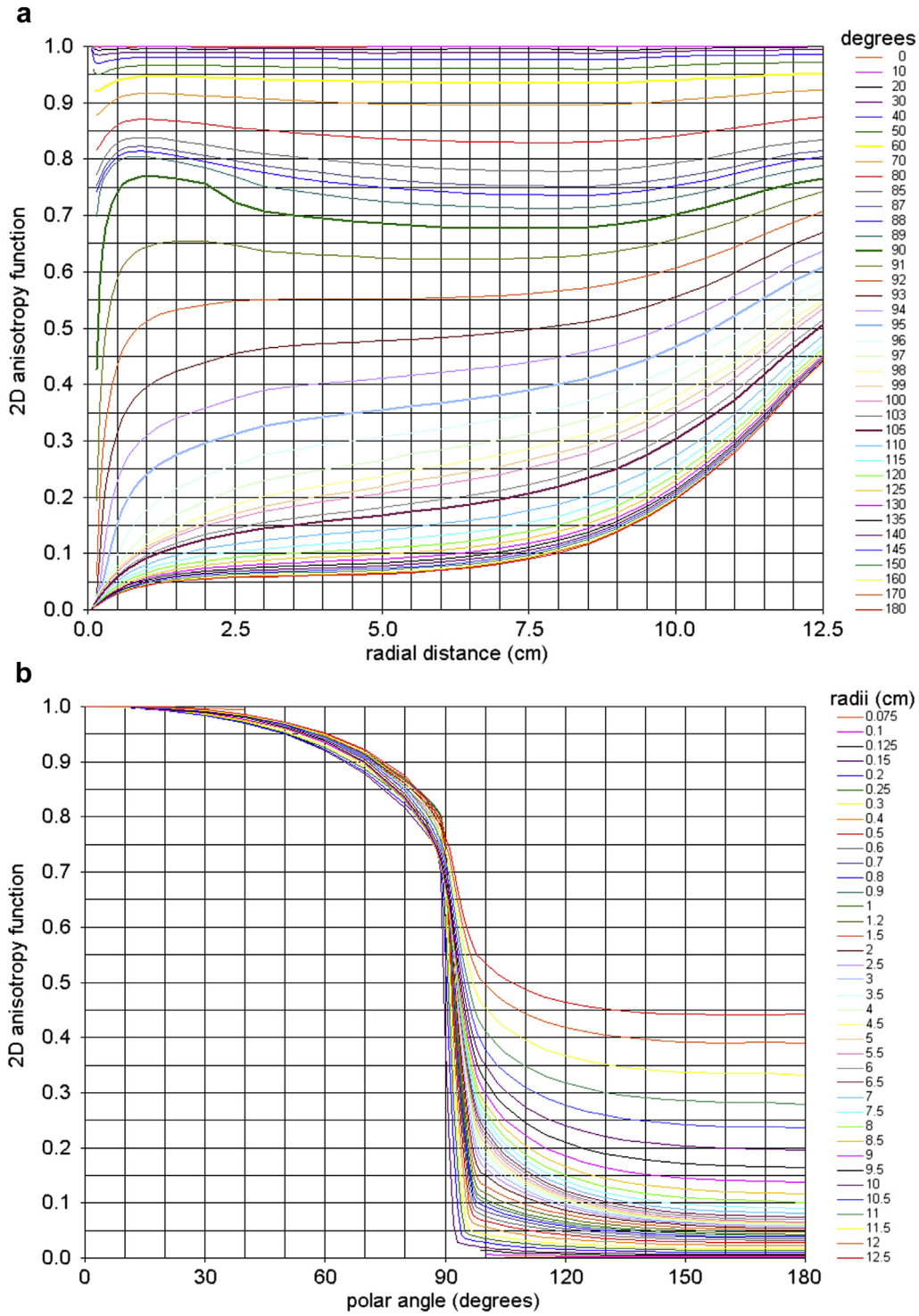

Fig. 4. Two-dimensional anisotropy function for the ^{103}Pd CivaDot brachytherapy source with the reference 35% Pd loading, normalized to unity at $\theta = 0°$ for (a) varying angles and (b) varying radii. The high gradient near the source (small r) and transverse plane ($\theta \sim 90°$) is evident, where the largest gradient was observed at $p(0.15\text{ cm}, \theta = 92°)$. Compared to conventional LDR low-energy seeds, these results were more uniform as a function of r. LDR = low dose rate.

2% over the majority region of clinical interest (Fig. 6). This was evident for distances up to 7 cm where statistical uncertainties increasingly contributed to the comparison. Near the CivaSheet periphery, radiation scatter was less with the superposition of single CivaDots and resulted in lower dose estimates by about 10%. Comparisons (not shown) of dose distributions for 6 × 12 and 6 × 18 arrays resulted in similar agreement within a few percent.

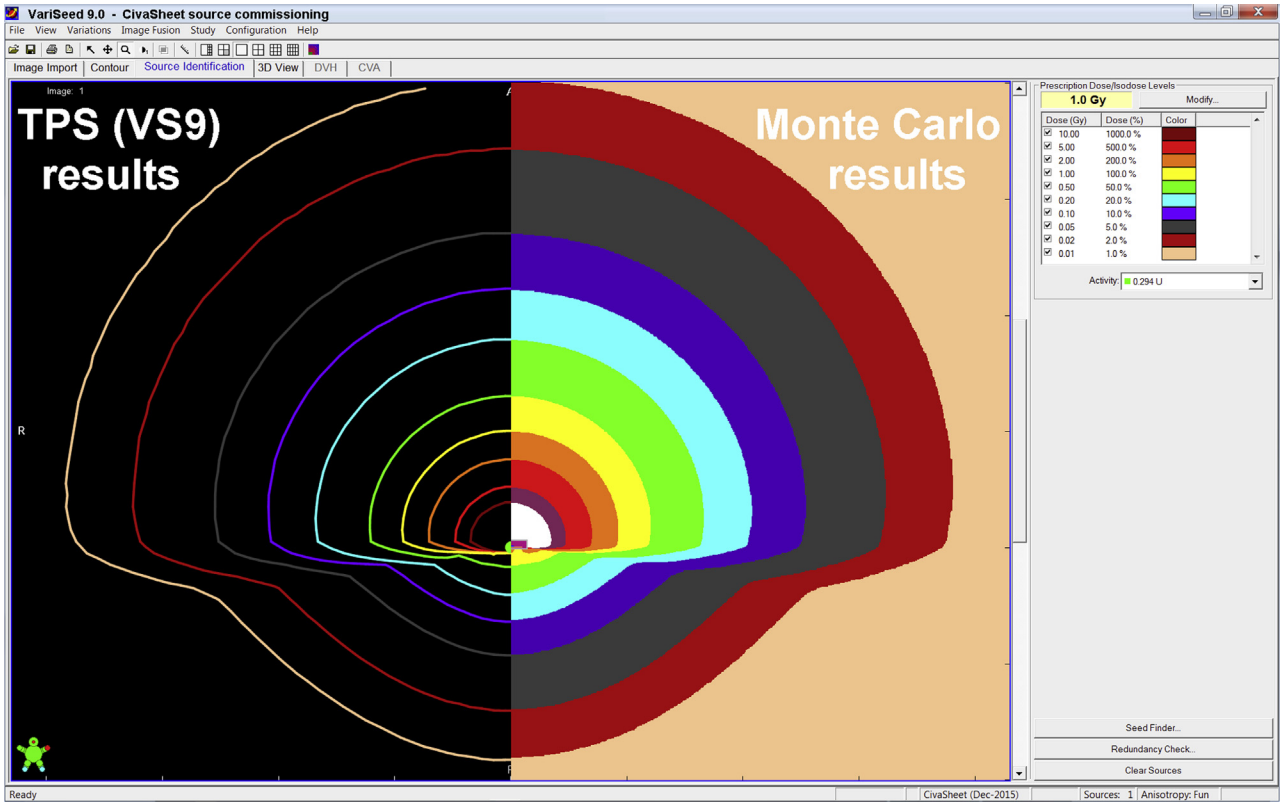

Fig. 5. Comparison of the isodose distribution from the VariSeed 9.0 treatment planning system (left) to the overlaid Monte Carlo–derived isodose distribution (right) for a commissioned CivaDot. A distance scale with centimeter increments is at the bottom with the lowest isodose level (1.0%) being about 8 cm wide.

Discussion

Dosimetry parameters and observations

Contributions by the Au L-shell characteristic x-rays to s_K (Fig. 2) increased its value while having minimal influence on the dose rate at 1 cm from the source. Consequently, the Λ value (0.579 ± 0.017 cGy h^{-1} U^{-1}) was lower in comparison to values for other ^{103}Pd BT sources, which are typically about 0.68 cGy h^{-1} U^{-1} when not containing Au markers.

The $g_{MC}(r)$ data (Fig. 3) were consistent within a few percent for the different loadings and in comparison to conventional ^{103}Pd seeds for $r \geq 1$ cm. Values for $g_{MC}(r)$ changed as expected for $r < 1$ cm due to spectral variations caused by self-shielding for different loadings and due to different physical distributions of the seeds and point-like CivaDots. Unless prescription doses are to differ substantially from those considered herein, it is not anticipated that clinics will use loading-specific parameters for BT dose calculations. The risks of confusion may rise above potential benefits.

The $F_{MC}(r,\theta)$ results (Fig. 4) exhibited behavior not observed for any other BT source where values near unity occur near $\theta = 90°$ and the lowest values occur near $\theta = 0°$. For the CivaSheet over $0° \leq \theta \leq 66°$, $F_{MC}(r,\theta)$ values were typically greater than 0.9, implying good dose uniformity in the forward direction toward $\theta = 0°$. Similarly, values over this range were nearly constant over all radii examined. With angles increasingly rearward (toward $\theta = 180°$) of the polar angle having the highest dose gradient (i.e., $\theta \sim 90°$), $F_{MC}(r,\theta)$ values increased with increasing radii due to increasing contributions of scattered dose from the unshielded directions.

^{103}Pd has a theoretical maximum specific activity of approximately 75 kCi/g, which is much higher than used by the manufacturer and incorporated into the simulations. Had such theoretically pure ^{103}Pd been used instead of the more dilute loadings assessed in the current study, factor of two loading variations as required by varying prescriptions would have had less of an affect on the dose distribution and resultant dosimetry parameters. Regardless, the effect of radionuclide loading has been similarly shown to have a small influence for other LDR ^{103}Pd BT sources (4, 38).

TPS data entry and TPS commissioning

Acquisition of the BT dosimetry parameters permits clinical treatment planning. Given the design differences between the CivaDot and conventional seeds (and subsequent need to develop an approach strictly differing from the TG-43 dose calculation formalism), it was rewarding to determine a solution compatible with the TPS dose calculation algorithm to permit accurate determination of the

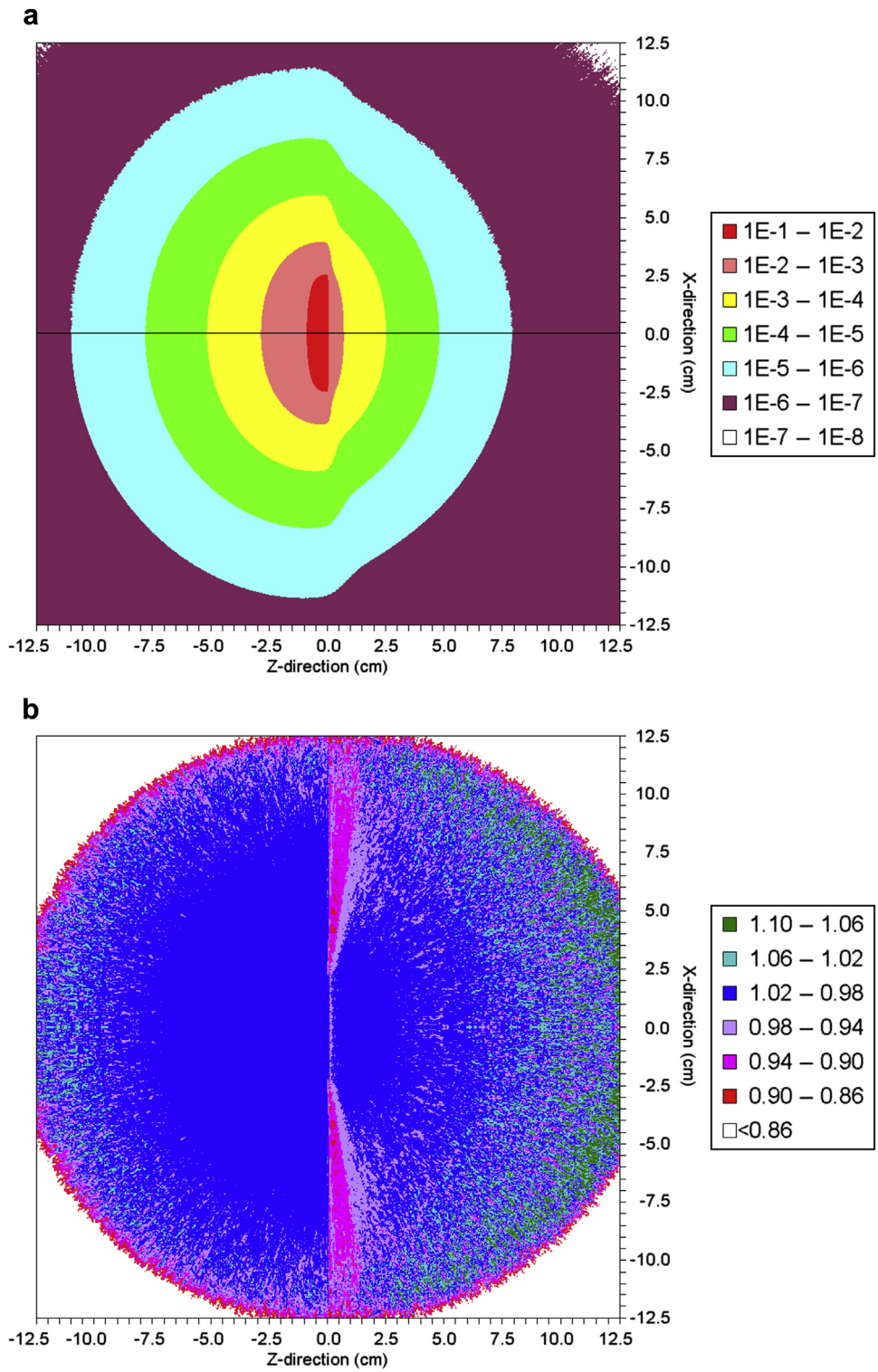

Fig. 6. (a) Comparison of the isodose distribution for a CivaSheet comprising a 6 × 6 array of CivaDots for Monte Carlo simulations (upper) and a test of the dose superposition principle when overlaying dose distributions for 36 CivaDots (lower) positioned at the same locations as in the CivaSheet array. Results are in MCNP6 native units (MeV/g/history) without normalizations or other corrections. (b) Ratio of the Monte Carlo simulation results to the dose superposition results. Results in the lower image are reflected on X = 0 due to geometric symmetry and to facilitate visual comparison with the isodoses depicted in part (a).

planned dose distribution. As a novel BT source, the process of TPS data entry and commissioning for the CivaDot was the same as for a conventional LDR BT seed (15). The simulation results were distilled into a data set that had linear and bilinear interpolation errors of $g_{TPS}(r)$ and $F_{TPS}(r,\theta)$ that were less than 2% for TPS entry. While a higher tolerance could

have been selected for generation of a smaller data set, this would not have substantially simplified the process of data entry or the TPS commissioning effort, or changed the outcome of the commissioning evaluation where one data point differed from the hand calculation by 3.1%.

There are no societal recommendations for the accuracy of the dose superposition principle as applied to BT dosimetry. However, comparisons of the simulated array of CivaDots comprising a CivaSheet with individual CivaDots located at the same positions as the 6 × 6 array were favorable with dose ratios typically within 1% in the high dose region and in contact with the shielded surface (39). These tests demonstrated that the approach is valid for the worse-case scenario with all the CivaDots on the same plane to maximize intersource shielding with resultant influence on radiation scatter. The accuracy realized by utilizing the dose superposition through geometric repositioning of CivaDots supersedes TPS limitations of intersource shielding and radiation scatter effects. Application of the dose superposition principle permitted image-guided clinical BT treatment planning and is more informative and patient specific than a nomogram.

Another clinically relevant finding was the uniformity of dose at depth in the treatment region for CivaSheets having arrays of 6 × 6, 6 × 12, or 6 × 18 CivaDots. The output uniformity over these arrays spanning a factor of three in area and source strength was within a few percent due to the short range of ^{103}Pd photon emissions where dose at a given location was dominated by the presence of a CivaDot with minimal contributions from distant sources. Consequently, it is suitable to trim the device in the operating theater to provide spatial conformity to the target without substantially diminishing the prescription dose (a function of total source strength) for depths ≤ 1.0 cm. This approach differs from the optimization and weighting of source strength necessary for sources such as interstitial BT implants with HDR ^{192}Ir where the high-energy photons have a larger range.

As for any new BT device, a robust evaluation should be performed that includes careful analysis of its dosimetry (15). Radiation oncologists should in advance have a good sense for the potential physical affect of the device, which is largely based on the dosimetry for BT sources. The current study contributes to such an evaluation by providing the tools to depict the radiation dose distribution, as well as indicating that differences between the TG-43 formalism for dose to water are small in comparison to the more realistic delivery of radiation dose to tissue. While differences increased with increasing distance from the source, this sensitivity to tissue composition was also observed for other ^{103}Pd BT sources (8, 40).

Potential limitations and weaknesses of the study

While simulations of ^{103}Pd dosimetry in low-Z carriers are well founded, the current study was based on simulations of radiation transport and potential misguided assumptions on the device geometry or radionuclide distribution would alter the findings. This is why it is necessary to complement simulations of BT dose distributions and subsequent derivation of dosimetry parameters with radiation dose measurements for low-energy photon-emitting BT sources, which are exquisitely sensitive to their design as shown by being the largest uncertainty component (Table 1) in this case. However, the overall uncertainty was less than is typically expected using measurements with thermoluminescent dosimeters or radiochromic film (4, 41).

The loading of 35% Pd by mass was based on measurements of the physical distribution of ^{103}Pd loaded by the manufacturer and the decayed specific activity at the time of device implantation. Covering the range of possible prescription doses, dosimetry parameters for several loading percentages were included as supplementary materials in support of clinical use if it is later found that this percentage loading was not correct or could be improved upon (Supplementary File 1).

Calibrations and disease sites

Preceding implantation, it is necessary to measure the source strength of CivaDots prepared from the same batch as those used to assemble the clinical implant (30). A custom source holder for a single CivaDot is available from Standard Imaging, Inc. (Middleton, WI) for the HDR 1000 plus reentrant well-type air ionization chamber. Clinical users must calibrate the combination of their chamber and the insert to obtain a NIST-traceable independent measurement of source strength. The maximum air-kerma strength of an individual CivaDot is 6.5 U, with a typical value of 2.6 U for delivering 120 Gy at a distance of 0.5 cm with 90% target coverage of the region covered by the CivaDot boundaries. A nomogram has been prepared to facilitate source ordering (Supplementary File 2) with values provided for D_{90} and D_{95} and target depths ranging from 0.1 to 1.0 cm where the treatment area is defined by the centers of the peripheral CivaDots.

To date, 12 patients have been treated with the CivaSheet at five institutions, where the TPS data were used for preimplant and postimplant treatment planning. The disease sites included colorectal, sarcoma, gynecologic, head and neck, and cancers of the axillary brachial plexus. Other prospective disease sites include lung, pancreas, and recurrent disease.

Device orientation documentation and imaging

It is important in the operating theater to ensure the CivaSheet is properly oriented due to the permanent nature of the implant and due to the radiation directionality. The shielded side is visibly evident by the Au shielding disks with the unshielded CivaDots appearing blue. Orientation

of the implanted CivaSheet can be documented before primary surgical closure through taking a photograph (care should be taken to preserve the sterile field) and illuminating the device with the bright surgical lights. This approach is necessary because the postimplant device orientation is not evident under high-resolution CT. The device is MRI compatible, but the CivaDots seem as black voids.

For postimplant imaging with CT to facilitate three dimensional (3D) image-guided treatment planning, the Au radio-opaque marker may be visualized with about 1 mm for slice thickness (based on an integer of the native scanning resolution) with a small field of view (about 2 cm larger in all directions than the implant extent but always ≥15 cm for preventing reconstruction artifacts). This will produce submillimeter voxels, which helps to minimize spatial uncertainties. Given the high-resolution slice thickness, the highest mAs and kVp settings will minimize image mottle and maximize x-ray production. A subsequent CT scan may be obtained using lower resolution for fusion with the high-resolution scan and for delineation of the entire volumes of adjacent organs-at-risk outside the prior tight field of view. Images may be obtained a week after implantation.

Treatment planning techniques and observations

The CivaDot dosimetry parameters have been used in the VariSeed, BrachyVision, and Oncentra BT TPSs. The following description is specific to the VariSeed 9.0 software, currently having the greatest experience, but the principles are applicable to any BT TPS. After acquisition of the CT, images are imported into the TPS and registered with segmented regions of interest that include the target and relevant healthy structures. The number of CivaDots implanted (noted in the operating theater) is used when identifying the positions of the CivaDots. The user may adjust the window/level setting to remove soft tissues, bony structures, and even surgical clips given the high-density high-Z Au markers. TPS auto-identification tools may facilitate this process. By then viewing the locations in various 3D views, a general sense is obtained of the implant geometry and relative positions of the CivaDots. While the maximum spacing between two adjacent CivaDots is 0.8 cm, this could seem as 1.1 cm if the scanning axis was aligned along the hypotenuse of the CivaSheet. Also, the minimum spacing could be only a couple millimeters if the CivaSheet was buckled during surgical implantation. Source orientation is a new tool to VariSeed 9.0, and the user can manipulate the source orientation through the combination of left mouse and Shift on the keyboard. By setting the TPS default to require use of the Ctrl key to place or delete sources, properly positioned sources will not disappear when orienting them in the sagittal and coronal views. This alignment is further facilitated by selecting a high isodose line (e.g., 500% of the prescription dose) to indicate the forward direction of the CivaDots and general knowledge of the CivaSheet orientation as documented from surgical placement. Orienting the CivaDots then is an iterative process between the 2D views permitting rotation and the 3D views depicting relative directions of each CivaDot. As for setting source positioning, the process of source orientation works best when anatomic imaging information does not occlude the sources. Images (Supplementary File 3) from a clinical implant depict visualization of CivaDots and soft tissue, along with isodose distributions and a comparison to a similarly prescribed theoretical implant with ^{103}Pd seeds at the same positions and orientations (Supplementary File 4).

For planar arrays, general properties were obtained for CivaSheet dosimetry (42). Misalignment of source positions away from the true distance by 0.1 cm altered target dose coverage by 15%, 7%, and 3%, at planar distances of 0.5, 0.7, and 1.0 cm, respectively. Lateral misalignment of source positions by 0.1 cm altered target dose coverage by 1.3%, 0.5%, and 0.1%, at the same planar distances. Misalignment of source orientation by 29°, 39°, and 56° altered target dose coverage by only 1%, 2%, and 5%, respectively, for target thicknesses ranging from 0.1 to 1.0 cm. For D_{90} target coverage and $d = 0.5$ cm (corresponding to 7.04 cm^3 for a 6 × 6 array), the V_{200}, V_{300}, V_{400}, and V_{500} values were 17%, 7.0%, 4.3%, and 2.9%, respectively. Up to $d = 0.7$ cm, sizing the CivaSheet may be reasonably performed by including the target within the peripheral CivaDot boundaries.

Areas for further research

Monte Carlo simulations and quantitative measurements of BT dose distributions are typically beyond the capabilities of most clinics and also not included in societal recommendations for source commissioning and quality assurance. However, calibration by the clinical medical physicist of single CivaDots (made from the same batch as the sterile CivaSheet ordered for the patient) is recommended (30).

To address the key uncertainty component identified in Table 1, it is possible to vary the Pd-loading percentage and measure its influence on S_K, the dose distribution in water, and sensitivity of the dosimetry parameters. While these types of measurements are challenging, fortunately the largest differences occur close to the source where radiation scatter is lowest, the dose rate is highest, and radiation detector signal is largest. For the loading range of 35% ± 15% included in the current study, variations in Λ and $g(r)$ are expected to be only a few percent. Given that measurements could be performed in a relative manner, several of the uncertainties constraining dose measurements may cancel. The approach taken by Aima *et al.* to alter the device design, such as through removal of the Au shielding disk (16), could be taken toward understanding the impact of Pd loading.

While not available to our knowledge, a mathematical model could be devised for the CivaSheet (analogous to an HDR TPS applicator library). Positions of all the CivaDots in a CivaSheet could then be determined given identification of a subset of the total, as well as to automatically determine the source orientation given assumption of sources being oriented normal to neighboring CivaDots.

Conclusions

Clinical treatment planning is now possible for the CivaSheet given availability of BT dosimetry parameters for use within TPSs. The combined uncertainties in these dosimetry simulations were less than 5%, with a similar magnitude for the influence of Pd loading on the dosimetry parameters. The practical aspects of commissioning the source in a clinical TPS were shown to be feasible and within the tolerance of societal recommendations. Dose superposition of CivaDots was shown to be an effective method to replicate the dose distribution of the CivaSheet.

Acknowledgments

This work was presented at the 2016 World Congress of Brachytherapy in San Francisco, CA, and supported in part by a research grant from CivaTech Oncology, Inc. The authors are grateful for discussions with Wes Culberson at the University of Wisconsin on the source coordinate system and the dose calculation methods, Michael Mitch at NIST for insight on developing procedures to accommodate this new directional source, and to Kristy Perez and Graeme O'Connell at CivaTech Oncology, Inc. for assisting with measurements of the source components.

Supplementary data

Supplementary data related to this article can be found at http://dx.doi.org/10.1016/j.brachy.2016.11.011.

References

[1] Aronowitz JN. Buried emanation: The development of seeds for permanent implantation. *Brachytherapy* 2002;1:167–178.
[2] Pérez-Calatayud J, Ballester F, Das RK, *et al*. Dose calculation for photon-emitting brachytherapy sources with average energy higher than 50 keV: Report of the AAPM and ESTRO. *Med Phys* 2012; 39:2904–2929.
[3] Aronowitz JN. Don Lawrence and the "k-capture" revolution. *Brachytherapy* 2010;9:373–381.
[4] Rivard MJ, Coursey BM, DeWerd LA, *et al*. Update of AAPM Task Group No. 43 Report: A revised AAPM protocol for brachytherapy dose calculations. *Med Phys* 2004;31:633–674.
[5] Rivard MJ, Butler WM, DeWerd LA, *et al*. Supplement to the 2004 update of the AAPM Task Group No. 43 Report: A revised AAPM protocol for brachytherapy dose calculations. *Med Phys* 2007;34: 2187–2205.
[6] Beyer DC, Puente F, Rogers KL, *et al*. Prostate brachytherapy: Comparison of dose distribution with different ^{125}I source designs. *Radiol* 2001;221:623–627.
[7] Meigooni AS, Awan SB, Rachabatthula V, *et al*. Treatment planning consideration for prostate implants with the new linear RadioCoil ^{103}Pd brachytherapy source. *J Appl Clinl Med Phys* 2005;6:23–36.
[8] Rivard MJ, Reed JL, DeWerd LA. ^{103}Pd strings: Monte Carlo assessment of a new approach to brachytherapy source design. *Med Phys* 2014;41:011716. (11 pp.).
[9] Adams QE, Xu J, Breitbach EK, *et al*. Interstitial rotating shield brachytherapy for prostate cancer. *Med Phys* 2014;41:0517033. (11 pp.).
[10] Han DY, Webster MJ, Scanderbeg DJ, *et al*. Direction-modulated brachytherapy for high-dose-rate treatment of cervical cancer. I: Theoretical design. *Int J Radiat Oncol Biol Phys* 2014;89:666–673.
[11] Han DY, Safigholi H, Soliman A, *et al*. Direction-modulated brachytherapy for high-dose-rate treatment of cervical cancer. II: Comparative planning study with intracavitary and intracavitary-interstitial techniques. *Int J Radiat Oncol Biol Phys* 2016;96:440–448.
[12] Lin L, Patel RR, Thomadsen BR, *et al*. The use of directional interstitial sources to improve dosimetry in breast brachytherapy. *Med Phys* 2008;35:240–247.
[13] Chaswal V, Thomadsen BR, Henderson DL. Development of an adjoint sensitivity field-based treatment-planning technique for the use of newly designed directional LDR sources in brachytherapy. *Phys Med Biol* 2012;57:963–982.
[14] DeWerd LA, Huq MS, Das IJ, *et al*. Procedures for establishing and maintaining consistent air-kerma strength standards for low-energy, photon-emitting brachytherapy sources: Recommendations of the Calibration Laboratory Accreditation Subcommittee of the American Association of Physicists in Medicine. *Med Phys* 2004;31:675–681.
[15] Nath R, Rivard MJ, DeWerd LA, *et al*. Guidelines by the AAPM and GEC-ESTRO on the use of innovative brachytherapy devices and applications: Report of Task Group 167. *Med Phys* 2016;43:3178–3205.
[16] Aima M, Reed JL, DeWerd LA, *et al*. Air-kerma strength determination of a new directional ^{103}Pd source. *Med Phys* 2015;42:7144–7152.
[17] Goorley T, James M, Booth T, *et al*. Initial MCNP6 release overview. *Nucl Technol* 2012;180:298–315.
[18] Wierzbicki JG, Rivard MJ, Waid DA, *et al*. Calculated dosimetric parameters of the IoGold ^{125}I source Model 3631-A. *Med Phys* 1998; 25:2197–2199.
[19] Reed JL, Rivard MJ, Micka JA, *et al*. Experimental and Monte Carlo dosimetric characterization of a 1 cm ^{103}Pd brachytherapy source. *Brachytherapy* 2014;13:657–667.
[20] Ballester F, Carlsson Tedgren Å, Granero D, *et al*. A generic high-dose-rate ^{192}Ir brachytherapy source for evaluation of model-based dose calculations beyond the TG-43 formalism. *Med Phys* 2015;42: 3048–3062.
[21] Rivard MJ. Monte Carlo radiation dose simulations and dosimetric comparison of the model 6711 and 9011 ^{125}I brachytherapy sources. *Med Phys* 2009;36:486–491.
[22] Available at: https://www-nds.iaea.org/public/download-endf/ENDF-B-VI-8/, International Atomic Energy Agency Nuclear Data Services, Vienna, Austria. Accessed November 9, 2016.
[23] NUDAT 2.6, National Nuclear Data Center, Brookhaven National Laboratory. Available at: http://www.nndc.bnl.gov/nudat2/reCenter.jsp?z=46&n=57. Accessed November 9, 2016.
[24] De Frenne D. Nuclear data sheets for A=103. *Nucl Data Sheets* 2009;110:2081–2256.
[25] ICRU Tissue substitutes in radiation dosimetry and measurement, International Commission on Radiation Units and Measurements Bethesda (ICRU 44, Bethesda, MD, 1989).
[26] Hubbell JH, Seltzer SM. Tables of x-ray mass attenuation coefficients and mass energy-absorption coefficients (version 1.4) 2004. [Online] Available at: http://physics.nist.gov/xaamdi National Institute of

Standards and Technology, Gaithersburg, MD. Accessed November 9, 2016.

[27] Rivard MJ. A discretized approach to determining TG-43 brachytherapy dosimetry parameters: Case study using Monte Carlo calculations for the MED3633 ^{103}Pd source. *Appl Radiat Isot* 2001;55:775–782.

[28] Rivard MJ, Evans D-AR, Kay I. A technical evaluation of the Nucletron FIRST® system: Conformance of a remote afterloading brachytherapy seed implantation system to manufacturer specifications and AAPM Task Group report recommendations. *J Appl Clin Med Phys* 2005;6:22–50.

[29] Rivard MJ, Granero D, Pérez-Calatayud J, *et al*. Influence of photon energy spectra from brachytherapy sources on Monte Carlo simulations of kerma and dose rates in water and air. *Med Phys* 2010;37:869–876.

[30] Butler WM, Bice WS Jr, DeWerd LA, *et al*. Third-party brachytherapy source calibrations and physicist responsibilities: Report of the AAPM low energy brachytherapy source calibration working group. *Med Phys* 2008;35:3860–3865.

[31] Rivard MJ, Melhus CS, Granero D, *et al*. An approach to using conventional brachytherapy software for clinical treatment planning of complex, Monte Carlo-based brachytherapy dose distribution. *Med Phys* 2009;36:1968–1975.

[32] Fraass B, Doppke K, Hunt M, *et al*. American Association of Physicists in Medicine Radiation Therapy Committee Task Group 53: Quality assurance for clinical radiotherapy treatment planning. *Med Phys* 1998;25:1773–1829.

[33] Williamson JF, Coursey BM, DeWerd LA, *et al*. On the use of apparent activity (A_{app}) for treatment planning of ^{125}I and ^{103}Pd interstitial brachytherapy sources: Recommendations of the American Association of Physicists in Medicine Radiation Therapy Subcommittee on low-energy brachytherapy source dosimetry. *Med Phys* 1999;26:2529–2530.

[34] *NRC Information Notice 2009-17*. Washington, DC: U.S. Nuclear Regulatory Commission; 2009. Available at: http://www.nrc.gov/docs/ML0807/ML080710054.pdf. Accessed November 8, 2016.

[35] Nath R, Anderson LL, Luxton, *et al*. Dosimetry of interstitial brachytherapy sources: Recommendations of the AAPM radiation Therapy Committee Task Group No. 43. American Association of Physicists in Medicine. *Med Phys* 1995;22:209–234.

[36] Rivard MJ, Beaulieu L, Mourtada F. Enhancements to commissioning techniques and quality assurance of brachytherapy treatment planning systems that use model-based dose calculation algorithms. *Med Phys* 2010;37:2645–2658.

[37] DeWerd LA, Ibbott GS, Meigooni AS, *et al*. A dosimetric uncertainty analysis for photon-emitting brachytherapy sources: Report of AAPM Task Group No. 138 and GEC-ESTRO. *Med Phys* 2011;38:782–801.

[38] Williamson JF. Monte Carlo modeling of the transverse-axis dose distribution of the model 200 ^{103}Pd interstitial brachytherapy source. *Med Phys* 2000;27:643–654.

[39] Melhus CS, Mikell JK, Frank SJ, *et al*. Dosimetric influence of brachytherapy seed spacers for permanent prostate brachytherapy. *Brachytherapy* 2014;13:304–310.

[40] Landry G, Reniers B, Pignol J-P, *et al*. The difference of scoring dose to water or tissues in Monte Carlo dose calculations for low energy brachytherapy photon sources. *Med Phys* 2011;38:1526–1533.

[41] Chiu-Tsao S-T, Napoli JJ, Davis SD, *et al*. Dosimetry for ^{131}Cs and ^{125}I seeds in Solid Water phantom using radiochromic EBT film. *Appl Radiat Isot* 2014;92:102–114.

[42] Rivard MJ, Rothley D. Treatment planning observations for the CivaSheet directional brachytherapy device using VariSeed 9.0. *Med Phys* 2016;43:3475. [abstract)].